How to cite: Angew. Chem. Int. Ed. 2024, e202408668
doi.org/10.1002/anie.202408668

Heterogeneous Catalysis

Surface Carbon Formation and its Impact on Methane Dry Reforming Kinetics on Rhodium-Based Catalysts by Operando Raman Spectroscopy

Riccardo Colombo[+], Gianluca Moroni[+], Chiara Negri, Guusje Delen, Matteo Monai, Alessandro Donazzi, Bert M. Weckhuysen, and Matteo Maestri**

Abstract: A mechanism for carbon deposition and its impact on the reaction kinetics of Methane Dry Reforming (MDR) using Rhodium-based catalysts is presented. By integrating Raman spectroscopy with kinetic analysis in an operando-annular chemical reactor under strict chemical conditions, we discovered that carbon deposition on a $Rh/\alpha\text{-}Al_2O_3$ catalyst follows a nucleation-growth mechanism. The dynamics of carbon aggregates at the surface is found to be ruled by the CO_2/CH_4 ratio and the inlet CH_4 concentration. The findings elucidate the spatiotemporal development of carbon aggregates on the catalyst surface and their effects on catalytic performance. Furthermore, the proposed mechanism for carbon formation shows that the influence of CO_2 on MDR kinetics is an indirect result of carbon accumulation over time frames exceeding the turnover frequency, thus reconciling conflicting reports in the literature regarding CO_2's kinetic role in MDR.

Methane Dry Reforming (MDR) is gaining both scientific and industrial interest as it is considered as one of the promising valorization routes of CO_2 to produce syngas (CO/H_2 mixture).[1] The MDR reaction is also of special interest when considering the production of fuels from biogas (a mixture of CO_2 and CH_4).[2] CH_4 and CO_2 react according to the following stoichiometry:

$$CH_4 + CO_2 \leftrightarrow 2\ CO + 2\ H_2 \quad \Delta H^0_{298K} = 247\ kJ/mol \qquad (1)$$

[*] R. Colombo,[+] Dr. G. Moroni,[+] Dr. C. Negri, Prof. Dr. A. Donazzi, Prof. Dr. M. Maestri
Laboratory of Catalysis and Catalytic Processes, Dipartimento di Energia, Politecnico di Milano, Via La Masa 34, 20156, Milano (Italy)
E-mail: matteo.maestri@polimi.it
Dr. G. Delen, Dr. M. Monai, Prof. Dr. Ir. B. M. Weckhuysen
Inorganic Chemistry and Catalysis Group, Institute for Sustainable and Circular Chemistry and Debye Institute for Nanomaterials Science, Utrecht University, Universiteitsweg 99, 3584 CG Utrecht (The Netherlands)
E-mail: m.monai@uu.nl
[+] These authors contributed equally to the work.

A major challenge in the MDR process is the need for stable catalysts resistant to deactivation by carbon deposits.[2c,3] In fact, carbon deposits can cover the catalyst active sites, thus leading to the deactivation of catalyst materials even in very short times (min–h).[4] Moreover, the extent of the carbon deposition is found to evolve over time and space in the reactor. Despite their high costs, noble metals offer remarkable reforming activity. However, carbon deposition has been found to occur also on noble metals, even if with characteristic times much higher than the ones of transition metals.[5] This makes noble metals perfect candidates for mechanistic studies because of the possibility of identifying the phases involved in the deactivation process. Among all, Rh has shown the best performances when supported on alumina and for this reason, a 4 % $Rh/\alpha\text{-}Al_2O_3$ catalyst has been used in this study.[5b,6]

The mechanism of carbon formation and its kinetic consequences on the reaction rate are still under debate and there is a clear need for unraveling the relationship between operating conditions, i.e., the carbon deposition rate, its structure and composition, as well as the catalyst performance.[7] To this aim, the catalyst material must be assessed in terms of conversion or yield during the reaction by online gas chromatography or mass spectrometry, while its active phase, including the involved active sites, must be simultaneously monitored with spectroscopy and/or microscopy. This is done in an attempt to correlate the changes in the catalyst composition and structure with the variations of the catalyst performance, including activity, selectivity, and stability.[8] This fundamental approach requires a simultaneous collection of reliable kinetic data (i.e., in a strict chemical regime) and relevant operando spectroscopic information.[9] The combination of such techniques allows for the acquisition of a comprehensive picture of the working catalyst at different length scales (from the nanoscale of the active phase at the nanoparticle level to the macroscale of the chemical reactor), which is pivotal to unravel the relationship between the phenomena at the level of the active sites and the activity of the entire reaction system.[10]

In this work, we have applied a multi-scale analytical approach, to relate characterization data with kinetic measurements in a strict chemical regime in an operando-annular chemical reactor.[9] More specifically, to gather insights into carbon deposition and structural changes of the catalyst during the reaction, operando Raman spectroscopy

was used to characterize the structure and composition of the carbon deposits, making it possible to discriminate whether they are perfectly graphitic or defective structures on the basis of the relative intensities of the G and D bands, respectively.[11] Ex situ analysis was conducted on the catalyst materials to characterize the samples both before and after the reaction. This analysis provided essential details about the morphology of the coke deposits formed during MDR. In particular, X-ray Diffraction (XRD) allowed to gain insights into the level of crystallization of carbonaceous deposits and into the presence of amorphous carbon.[12] Scanning Electron Microscopy (SEM) and Transmission Electron Microscopy (TEM) provided fundamental information about the size of Rh metal nanoparticles, to assess the role of sintering in the catalyst deactivation, as well as the form of carbon deposits (organized either in encapsulating film or filaments).[13] Photo-induced Force Microscopy (PiFM) was also applied to provide additional information on the structure and composition of the coke deposits and assess their distribution at the nanoscale on the catalyst surface.[14] The collection of kinetic data combined with the spectroscopic information at different lengths and time scales led us to propose a plausible mechanism for carbon formation and growth during MDR on Rh, which is valid under a wide range of operating conditions, and to relate the catalyst performance with the carbon deposition dynamics at the active site. The obtained mechanistic insights allowed also to resolve apparent contradictions in the literature on the kinetic role of CO_2 in the MDR process.[15]

We monitored the catalyst activity and selectivity for time-on-stream (TOS) up to 140 h for different conditions of CO_2/CH_4 ratio and inlet CH_4 concentrations over 4 wt% $Rh/\alpha\text{-}Al_2O_3$ catalyst in an annular reactor (the experimental methods are reported in Section S1 and S2 of the Supporting Information). The products' distribution obtained in the experimental tests was in accordance with the stoichiometry of the MDR reaction (Eq. 1). Only for CO_2/CH_4 ratios higher than 2 the contribution from the reverse-Water Gas Shift (r-WGS) became evident (Figure S5). Figure 1a shows CH_4 conversion over 140 h of reaction at 600 °C for inlet $CH_4 = 8$ vol.% and 1 vol.% at CO_2/CH_4 ratio equal to 1. The experiments revealed a descending trend over time in methane conversion. For instance, in the case of $CH_4 =$ 8 vol.%, CH_4 conversion decreased from 47 % at time-on-stream (TOS) = 0.1 h to 37 % after 6 h. Then, the variation of CH_4 conversion over time was substantially reduced. Indeed, during the following 12 h (from TOS 6 h to 18 h) the conversion decreased to 34 %. As such, the conversion decay continued progressively even if with a lower time-derivate: the CH_4 conversion was still 33 % after 24 h and 30 % after 72 h. Finally, it reached 27.5 % after 140 h determining a total 19.5 % loss. Overall, the characteristic time of the time-evolution of catalyst activity was much higher (h) than the characteristic time of the turnover rate(s), thus making it evident that the catalyst is undergoing a deactivation process. For the test conducted at $CH_4 = 1$ vol.%, the time-variation of conversion was analogous but less pronounced; indeed, conversion dropped from an initial 77 % to 71.5 %

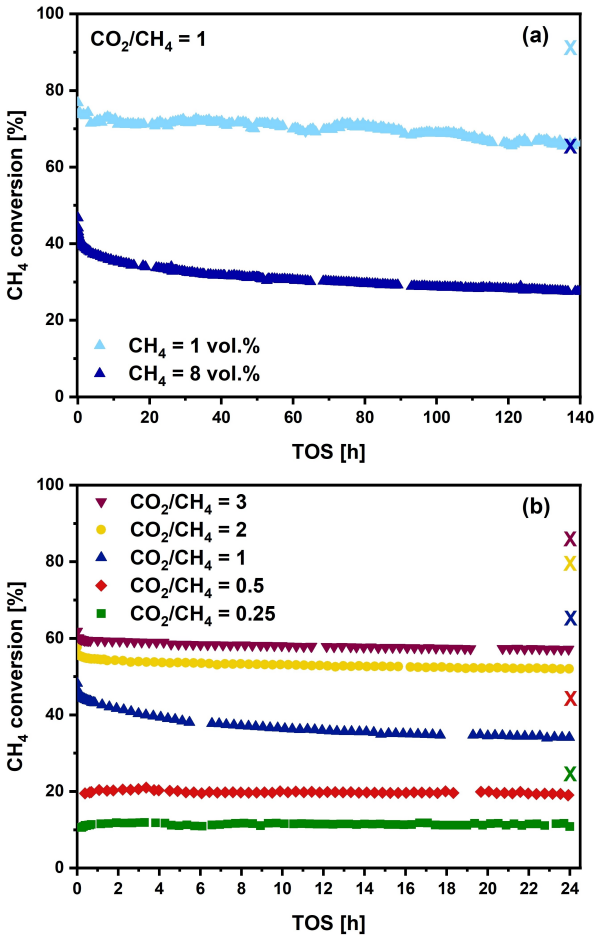

Figure 1. Catalyst activity and stability monitored in terms of methane conversion (symbols) during methane dry reforming (MDR) over 4 wt% $Rh/\alpha\text{-}Al_2O_3$.%, with respective equilibrium conversion ("X" symbols): (a) 140 h stoichiometric CO_2/CH_4 tests for inlet $CH_4 = 1$ vol.% and $CH_4 = 8$ vol.%; (b) 24 h tests at different CO_2/CH_4 ratios and inlet $CH_4 = 8$ vol.%. Conditions: T = 600 °C, P = 1 atm, Gas-Hourly Space Velocity (GHSV) = 1400 [L(STP)/g_{cat}/h].

after 6 h and reached 66 % after 140 h for a cumulative 11 % loss. Figure 1b shows the influence of the CO_2/CH_4 ratio on the time-evolution of the conversion during $CH_4 = 8$ vol.% MDR tests. For $CO_2/CH_4 > 1$ the decrease of the methane conversion over time was less pronounced than the dynamics observed for the $CO_2/CH_4 = 1$. For instance, for the $CO_2/CH_4 = 2$ test, the initial conversion was 57.5 % which decreased to 53.5 % after 6 h, and then to 52 % after 24 h for a total 5.5 % loss. This contrasts with the more significant reduction of 10 % (from 47 % to 37 %) in the first 6 h, followed by a 4 % loss (from 37 % to 33 %) in the following 18 h for $CO_2/CH_4 = 1$. For CO_2/CH_4 ratios below 1, such as 0.5 and 0.25, methane conversion remained stable over time, showing no dynamic change over TOS. Thus, it is clear that the CO_2/CH_4 ratio significantly affects the dynamics of methane conversion.

While examining the catalyst activity, we monitored the surface of the catalyst material using operando Raman spectroscopy for the whole series of operating conditions of

Figure 1. Specifically, Figure 2 presents time-resolved Raman spectra taken at the end of the catalytic bed during tests with an inlet methane concentration of 8 vol.% under various CO_2/CH_4 ratios. When using an over-stoichiometric CO_2/CH_4 ratio of 2, the Raman spectra over a 24-h period showed no carbon peaks (as seen in Figure 2a). In contrast, at a $CO_2/CH_4=1$ stoichiometric ratio, Raman bands related to carbon deposits appeared within 3 h of reaction time (Figure 2b). We observed the G-band at ~1580 cm^{-1}, indicative of sp^2, graphitic carbon (with a possible small contribution of the defect *D′*-band at ~1620 cm^{-1}), and the defect-related D-band at ~1350 cm^{-1}.[16] For CO_2/CH_4 ratios below 1, the G and D Raman bands were detectable after just 5 min of reaction (Figures 2c and 2d). The Raman bands grew in intensity over time, particularly for CO_2/CH_4 lower than 1, where the G Raman band became more pronounced. The evolution of the intensities of these Raman bands over time was also influenced by the methane concentration, as demonstrated by tests with a 1 vol.% CH_4 concentration (Figure S7). Notably, at any given CO_2/CH_4 ratio, the intensities of the G and D bands were consistently lower compared to what was observed in tests with a higher methane molar fraction, indicating that the amount of carbon deposited was less at lower CH_4 inlet concentrations.

To gain insights into the mechanism of carbon deposition, we monitored the spatial resolution of the Raman spectra along the reactor. Figures 3a and 3b show the spatially resolved spectra collected after 24 h and 140 h of TOS for the test at inlet $CH_4=8$ vol.% and $CO_2/CH_4=1$. For each spatially resolved scan, five Raman spectra were collected every 5 mm along the reactor axial coordinate, from the reactor entrance to the reactor outlet, namely from position 1 to position 5. These spectra, which have been vertically shifted to point out more clearly any possible differences in the spectroscopic features, clearly display the fingerprint bands related to carbonaceous species. After 24 h (Figure 3a) the carbon deposits were not uniformly distributed but stratified along the axial coordinate, decreasing from the inlet (position 1) to the outlet of the reactor (position 5). Subsequently, peak intensities in the first half of the reactor (positions 1 and 2) showed negligible differences after 140 h (Figure 3b), while the others (positions 3, 4, and 5) displayed a clear enhancement, especially for the G band, which became noticeably more intense than the D

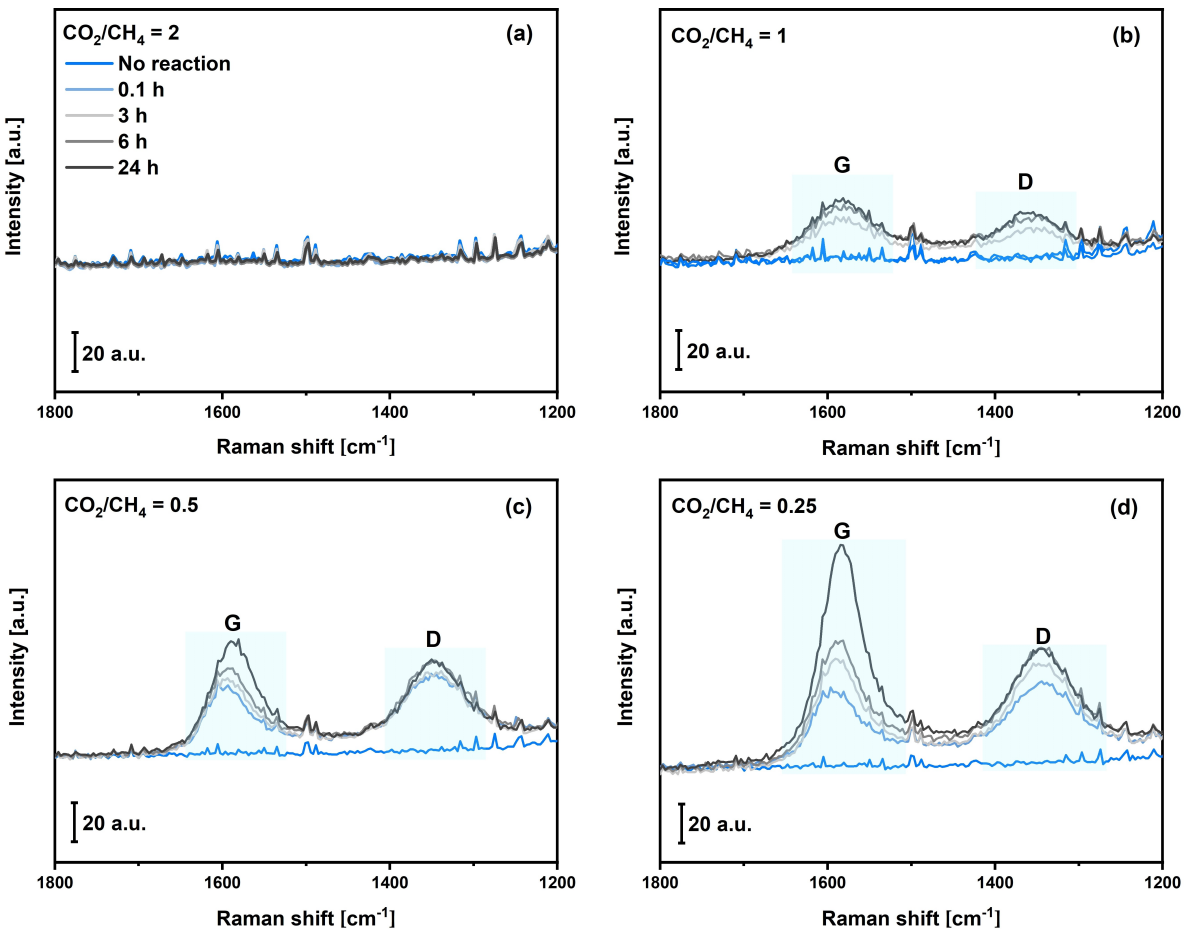

Figure 2. Time-resolved operando Raman spectra acquired with a Raman probe positioned at the end of the catalytic bed, at a time-on-stream (TOS) of 0.1 h, 3 h, 6 h and 24 h of Methane Dry Reforming (MDR) test over 4% Rh/Al_2O_3 catalyst for inlet $CH_4=8$ vol.% at different CO_2/CH_4 ratios $CO_2/CH_4=2$ (a), 1 (b), 0.5 (c) and 0.25 (d). The spectra are compared to the Raman spectrum of a fresh catalyst. Conditions: T = 600 °C, P = 1 atm, Gas-Hourly Space Velocity (GHSV) = 1400 [L(STP)/g_{cat}/h].

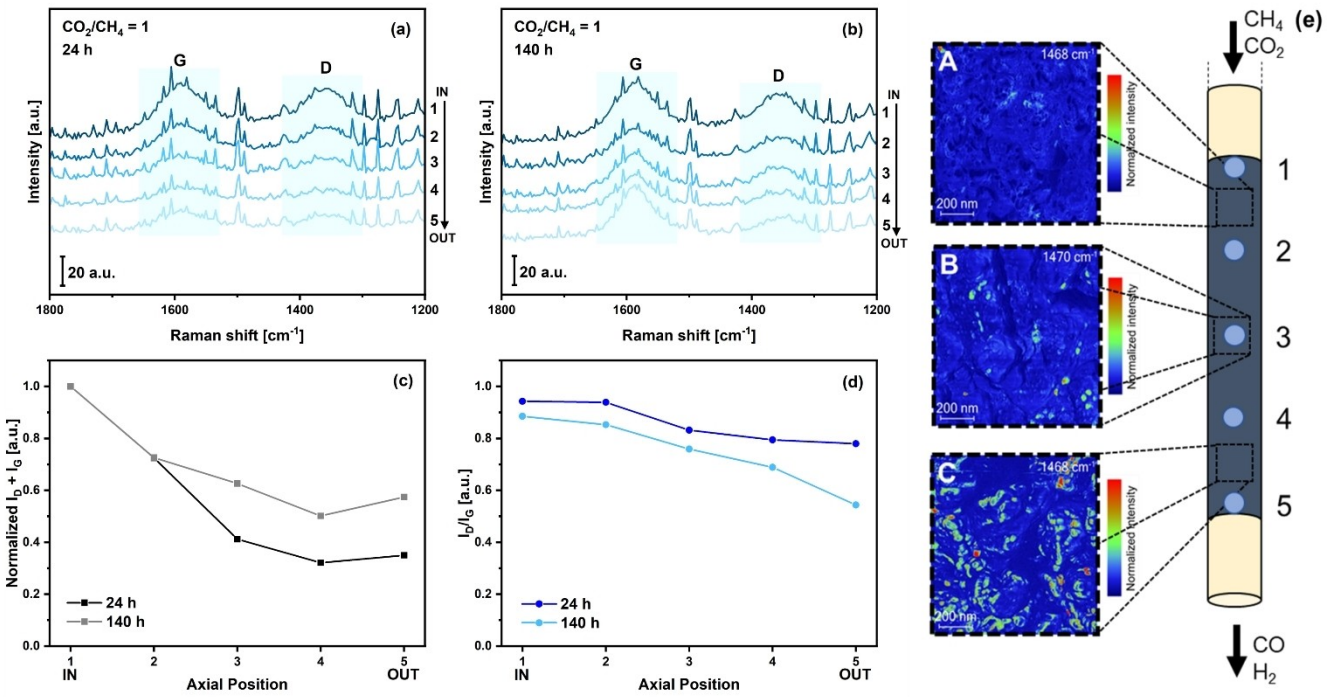

Figure 3. Spatially resolved operando Raman spectra acquired during a Methane Dry Reforming (MDR) test at a time-on-stream (TOS) of 24 h (a) and 140 h (b), over a 4% Rh/Al_2O_3 catalyst, for inlet $CH_4 = 8$ vol.% at $CO_2/CH_4 = 1$. Conditions: T = 600 °C, P = 1 atm, Gas-Hourly Space Velocity (GHSV) = 1400 [L(STP)/g_{cat}/h]. Position 1: reactor entrance, position 5: reactor outlet, one position every 5 mm. Panel (c) shows the axial profile of the sum of the G and D Raman band intensities normalized by the value in position 1 (reactor entrance) (black TOS = 24 h, grey TOS = 140 h). In panel (d), the I_D/I_G ratio is depicted as a function of reactor length (blue TOS = 24 h; light blue TOS = 140 h). (e) Ex situ photo-induced force microscopy (PiFM) conducted on a spent 4% Rh/Al_2O_3 catalyst after 8 h MDR at $CO_2/CH_4 = 1$ at 600 °C. The 1468–1470 cm^{-1} band was chosen to observe spatial mapping of the breathing modes of hydrocarbon deposits.

band. The same considerations can be extended to the $CH_4 = 1$ vol.% test, except for a slower dynamic of carbon formation. Figure S9 shows that, after 24 h, no carbon Raman bands were detected along the reactor. However, after 140 h, carbon signals started to be detected in the first half of the reactor bed.

To more effectively emphasize the spatial resolution of the carbon deposits from a quantitative perspective, we have presented the spectra in Figure 3a and b as the sum of the G and D band intensities, normalized relative to the sum value at the reactor inlet (Figure 3c). The combined intensities of the G and D peaks after 24 h of TOS exhibited a decreasing trend along the reactor axis, showing a 60% reduction from the reactor inlet (position 1) to the reactor outlet (position 5). This trend was reversed at longer reaction times (TOS = 140 h), as the combined intensities of the G and D peaks increased more significantly in the latter half of the reactor (positions 3, 4, and 5), while positions 1 and 2 showed no changes compared to the measurements acquired after 24 hours. This phenomenon is linked to the observation that, over longer periods, the G band increased in intensity in the latter half of the reactor, as reported in Figures 3a and 3b.

These observations were further corroborated by the axial and temporal evolution of the integral intensity ratio of the D and G bands (I_D/I_G), recognized as an indicative measure of the carbon's graphitization level (Figure 3d).[17] An I_D/I_G value greater than 1 indicates a high level of structural disorder within the carbon structures, whereas a value less than 1 suggests the formation of highly graphitic carbonaceous materials. After 24 h, the I_D/I_G ratio was approximately 1 at the reactor inlet and decreased monotonically towards the outlet, reaching 0.8. After 140 h, the I_D/I_G ratio diminished across all reactor positions, particularly in the second half. Notably, at position 5 (reactor outlet), the I_D/I_G ratio dropped to 0.6, due to a significant increase in the intensity of the G band. As such, Figure 3d makes it evident that the formation of highly graphitic carbonaceous materials occurred at the end of the reactor. Analogous trends were observed both in terms of CH_4 conversion and Raman spectra at different space velocities (Figures S12 and S13) and temperatures (Figures S14, S15, and S16), showing the general relevance of our observations.

The findings from the spatially resolved operando Raman spectroscopy analysis were further corroborated by investigating carbon deposition on the catalyst surface after the test under $CH_4 = 8$ vol.% and $CO_2/CH_4 = 1$ using the PiFM technique.[18] The distribution and intensity of the IR signal at 1470 cm^{-1} (relative to C=C bending vibration and thus associated to graphitic coke deposits[19]) is presented in panels A, B and C of Figure 3e. The PiFM results indicate that coke spots associated with ordered carbon were more abundant towards the end of the catalytic bed, in accordance with the higher level of graphitization suggested by the I_D/I_G

parameter derived from the spatially resolved operando Raman spectroscopy data. Moreover, the PiFM maps show that carbonaceous species were not homogeneously formed along the catalyst bed but rather accumulated in islands on the catalyst surface.

The time and spatial evolution of the Raman spectra was dependent on the CO_2/CH_4 ratio. For instance, at $CO_2/CH_4 = 0.5$ and inlet $CH_4 = 8$ vol% (Figure 4a at TOS = 3 h and Figure 4b at TOS = 24 h), the evolution of the Raman bands was faster than for higher ratios. In fact, by presenting the spectra as the cumulative intensity of the G and D bands across the reactor, normalized to the intensity at the reactor's inlet, it was observed that at shorter TOS (3 h), the trend continued to decline, leveling off at extended TOS (24 h) due to the gradual accumulation of carbon on the surface. Additionally, the I_D/I_G ratio remained roughly constant (at about 1.2) throughout the reactor's length, suggesting a slightly more defective crystalline structure than for higher CO_2/CH_4 ratios.

To measure the dimensions of Rh nanoparticles and to evaluate any potential sintering effects contributing to deactivation, the catalyst material was also characterized ex situ following the reaction by TEM analysis (Figure S3). The particle size distributions of Rh nanoparticles for both the reduced fresh sample (Figure S3a) and the spent catalysts (Figures S4b, 4c, and 4d) were statistically similar, ~3.6–3.9 nm, with a standard deviation of 1.6–1.8 nm. This finding disproves sintering as a cause of deactivation. TEM images (Figure S4) further showed the formation of filamentous carbon nanostructures on some of the spent catalysts.[13,20] Such carbon filaments were observed in spent samples from tests with a CO_2/CH_4 ratio of 1 and 0.5 and inlet CH_4 concentration of 8 vol.%, whereas no carbon deposits were detected when the CO_2/CH_4 ratio was 2, aligning with the operando Raman spectroscopy results. Additionally, more carbon fibers were observed for the CO_2/CH_4 ratio of 0.5 by TEM (Figure S4), in accordance with the Raman spectra, shown in Figure 2c.

In summary, according to the ex situ characterization (PiFM and TEM) and the spatiotemporal operando Raman spectroscopy measurements filamentous, highly graphitic coke structures become more abundant as the CO_2/CH_4 ratio decreases. All in all, the active sites are subject to a dynamic evolution (order of hours of TOS) which is much

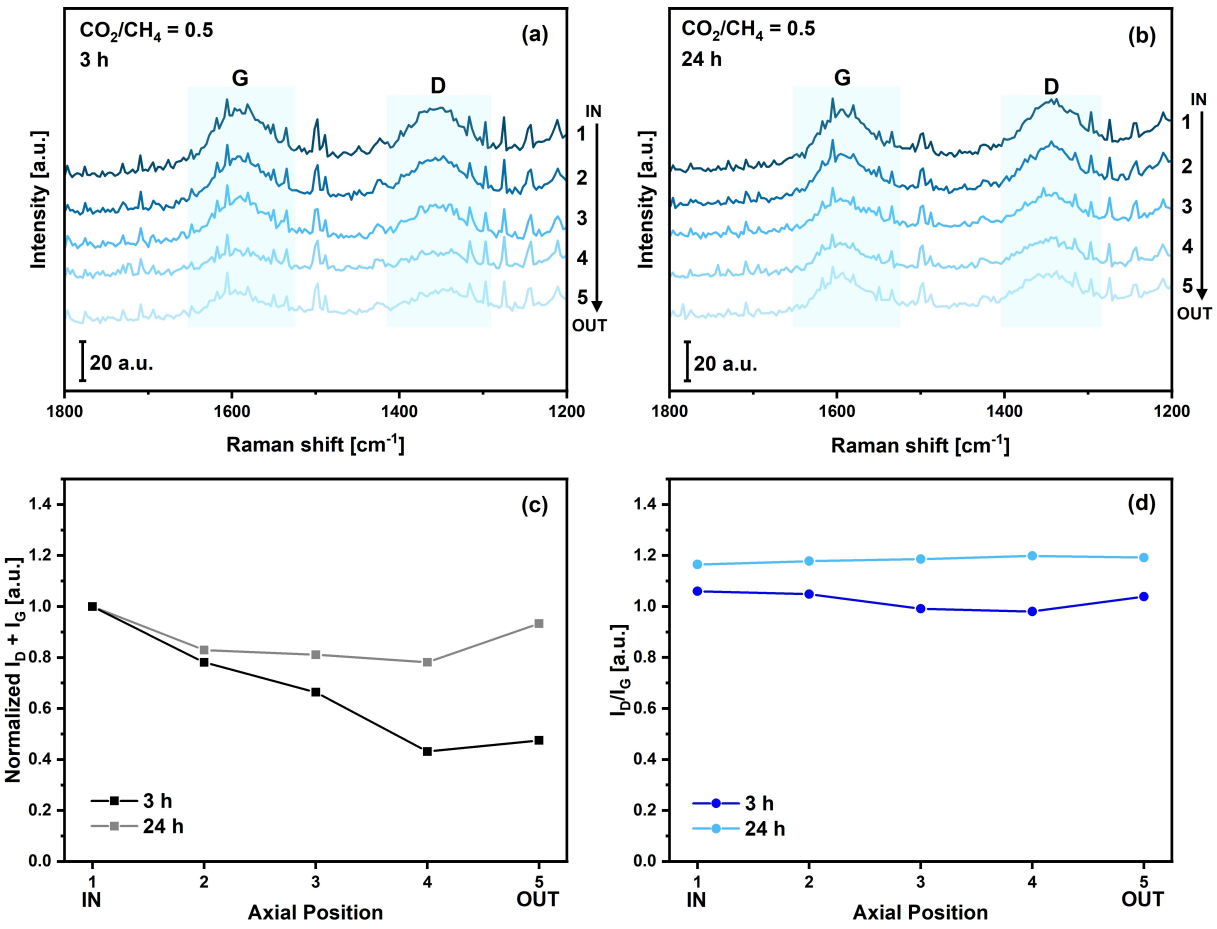

Figure 4. Spatially resolved operando Raman spectra during a Methane Dry Reforming (MDR) test, at a time-on-stream (TOS) of 3 h (a) and 24 h (b) over a 4% Rh/Al_2O_3 catalyst, for inlet $CH_4 = 8$ vol.% at $CO_2/CH_4 = 0.5$. Conditions: T = 600 °C, P = 1 atm, Gas-Hourly Space Velocity (GHSV) = 1400 [L(STP)/g_{cat}/h] Position 1: reactor entrance, position 5: reactor outlet, one position every 5 mm; (c) axial profile of the sum of the intensities of the Raman G and D bands, normalized by the value in position 1 (black TOS = 3 h, grey TOS = 24 h); and (d) corresponding I_D/I_G ratio (blue TOS = 3 h; light blue TOS = 24 h).

longer than the turnover rate of the catalytic cycle. For this reason, the catalytic cycle can reach a steady state condition at the level of the active site (i.e., the catalytic cycle). The amount of active sites available for the MDR reaction is affected by the slow dynamics ruled by carbon deposition, thus resulting in a deactivation process, as evident from the activity measurements over time. In particular, the fact that the carbon deposits are found to be decreasing, but becoming more graphitic, along the reactor length is in line with the fact that the catalyst fouling compound, C_{solid}, is formed by a reaction, which is parallel to the main reactions,[21] as represented in Scheme 1. As soon as the reactants are fed to the reactor, the catalytic cycle is established. On the one side, the reaction mechanism entails the decomposition of CH_4 into CH_x fragments and to C* species that are eventually oxidized to CO by means of the O provided by the CO_2 activation at the surface (Route 1 in Scheme 1).[15b,d,22] On the other hand, the CH_x fragments act as carbon precursors (Route 2 in Scheme 1). These species rearrange into benzene rings, becoming increasingly conjugated, leading to the formation of structured carbon-based species (i.e., mainly graphitic filaments as highlighted by Raman spectroscopy and TEM). The formation of the nuclei at the metal surface covers part of the active sites, thus leading to a reduction of the catalyst activity. As Rh nanoparticles become increasingly covered by carbonaceous nuclei, there is a gradual decrease in the observed activity over time-on-stream (Figure 1).

Once the carbon nuclei are formed, the difference in the CH_x* chemical potential between the free catalytic surface and the nuclei creates a migration of CH_x* intermediates towards the nuclei themselves which organize the intermediates in filaments that grow over the Rh nanoparticles, in full analogy with the base growth or tip growth mechanisms reported in the literature for Ni-based catalysts.[13,23] However, as shown in Figure S4, only a few Rh metal nanoparticles detached from the alumina support. This evidence indicates that a base growth mechanism for carbon filament formation is favored over Rh, in contrast to Ni.[7a] When the growth of carbon filaments prevails over the creation of new nucleation centers, the carbon deposition does not directly result in covering the active sites and thus the catalyst activity becomes less affected by the formation and growth of the carbon aggregates with a noticeable shift in the derivative of the CH_4 conversion relative to the TOS.[24] The preferential growth of ordered filamentous carbon species is also in line with the operando Raman spectroscopy measurements in which the intensities of the carbon bands, especially the G one, continued to increase over time without further compromising the catalyst activity to the same degree (Figures 1a and 3). In addition to the activity provided by the active sites remaining free from carbon aggregates, part of the observed activity could be also ascribed to non-metallic catalysis brought forth by the carbon itself. In fact, carbon deposits are reported to activate both CH_4[25] and CO_2.[26] In particular, CO_2 activation requires highly amorphous carbon deposits.[27] According to the XRD analysis (Figure S2), the peak at $2\theta = 32°$ can be ascribed to an amorphous carbon structure; nonetheless, as confirmed by the low values of the I_D/I_G ratios derived from Raman spectra (e.g., Figures 3d and 4d), most of carbonaceous species produced by the reaction are strongly organized structures with a high level of graphitization. Thus, we presume the possible contribution of non-metallic catalysis to be minor.[27]

To assess the kinetic consequences of the observed carbon deposits on the catalyst activity, we exploited the chemical removal of carbonaceous deposits via the reverse Boudouard reaction ($CO_2 + C \rightarrow 2\ CO$) by treating the spent catalysts at 750 °C using a stream of pure CO_2 (GHSV = $1*10^5$ Nl/kg_cat/h) for 90 min. Figure 5a illustrates the results of an MDR test (inlet $CH_4 = 8$ vol.% — $CO_2/CH_4 = 1$) followed by a treatment in pure CO_2 and again by the same MDR test. The regeneration process resulted in a complete reactivation of the catalyst at the start of the second MDR run, followed by a deactivation trend that was identical to the first test. Furthermore, as highlighted by Figure 5b, the Raman spectra post-CO_2 regeneration did not show any G and D bands. These findings conclusively link the deactivation process to the spatiotemporal buildup of carbon deposits on the catalyst.

Our mechanistic interpretation can explain how the extent and the duration of the observed catalyst dynamics are influenced by the CO_2/CH_4 ratio and the CH_4 concentration, as observed in Figure 1b and Figure S6. With methane as the precursor of the carbon aggregates, at a given CO_2/CH_4 ratio, an increase in CH_4 concentration leads to a higher chemical potential of the carbon aggregates, thereby accelerating the formation and growth of the carbon deposits. On the other hand, a higher CO_2/CH_4 ratio results in a CO_2-enriched local chemical environment, which tends to inhibit the growth of carbon aggregates in line with Figure 5. Conversely, a lower CO_2/CH_4 ratio leads to a CO_2-deficient local chemical environment at the active site. Such an environment does not hinder the formation and growth of carbon aggregates, thus speeding up the dynamics of the formation and growth of carbon aggregates during MDR. This aligns with the observation that for a CO_2/CH_4 ratio of 0.5, the nucleation and growth of carbon filaments occurred rapidly, resulting in well-pronounced G and D bands in the Raman spectra being visible at very short TOS (< 5 min). Consequently, the fast nucleation of C-nuclei leads to a deactivation that was too fast to be detected by the micro-

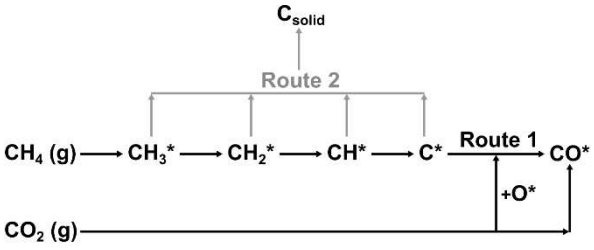

Scheme 1. Simplified pathways for C* adsorbed species. Route 2, responsible for solid carbon formation, is occurring in parallel to Route 1, which instead leads to Methane Dry Reforming (MDR) products yield.

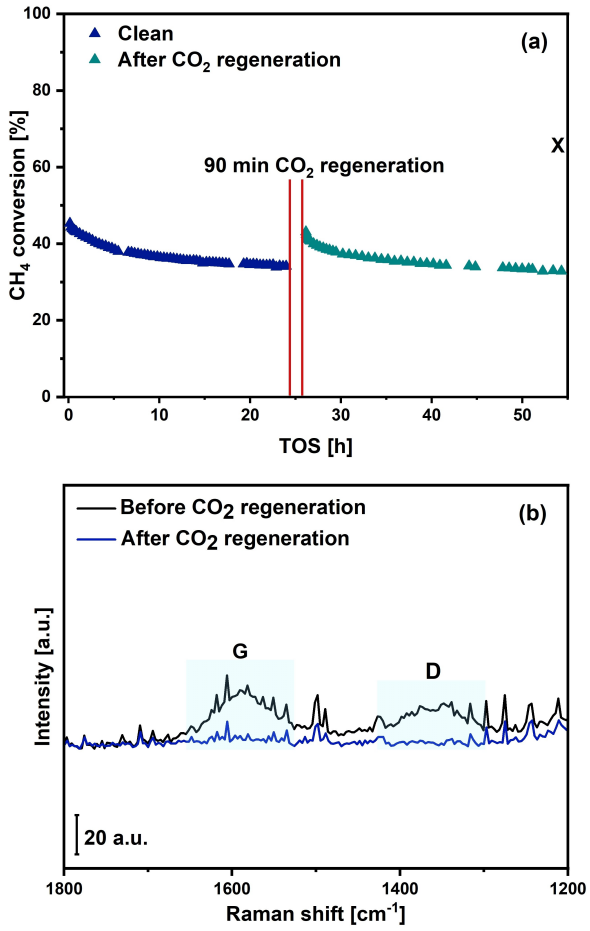

Figure 5. (a) Methane conversion during a 24 h Methane Dry Reforming (MDR) test at 600 °C over a 4 % Rh/Al_2O_3 catalyst for inlet $CH_4 = 8$ vol.% at $CO_2/CH_4 = 1$, followed by a 90 min CO_2 regeneration at 750 °C, and a second MDR run of 24 h. The respective thermodynamic equilibrium conversion is indicated by a "X" symbol. Conditions: T = 600 °C, P = 1 atm, Gas-Hourly Space Velocity (GHSV) = 1400 [L-(STP)/g_{cat}/h]; (b) operando Raman spectra acquired with a Raman probe positioned at the end of the catalytic bed before and after the CO_2-treatment.

GC instrumentation, thereby presenting an apparently constant conversion over 24 h (Figure 1b).

For additional validation of the proposed mechanism, we attempted to deliberately alter the growth of the C-deposits (C_{solid} in Scheme 1) by introducing a minor concentration of oxygen into the inlet gas mixture ($O_2 = 0.8$ %).[5c,15b] Figure 6a reveals that the initial conversion rates up to TOS = 0.2 h for $CO_2/CH_4 = 1$ were nearly identical in the presence or in the absence of O_2. This indicates that oxygen does not play a kinetic role in the reaction. For longer TOS, however, the introduction of oxygen reduced the rate of deactivation, with a CH_4 conversion of 42 % after 24 h, which was 9 % higher than in the test performed without oxygen. Such a difference in the rate of decline of conversion was associated with a different dynamic of accumulation of C-deposits at the surfaces, as evident by the corresponding operando Raman spectroscopy results (Figure 6b). In fact, no Raman bands were observed after 24 h of TOS, as opposed to the distinct Raman carbon bands observed in the absence of O_2 (compare Figure 6b and 2b). Such a slow-down of C deposition and growth dynamics explains the reduced rate of deactivation observed in Figure 6a. This effect is even more evident for $CO_2/CH_4 < 1$. For instance, for $CO_2/CH_4 = 0.5$, the addition of oxygen significantly slowed down the dynamics of the C-deposition at the surface, as evident from the collection of the Raman spectra along the reactor. In fact, in contrast with the test without co-feeding of oxygen (Figure 2c), in the presence of the co-feed of O_2 no carbon bands were detectable along the entire reactor after 6 h of reaction (Figure S11) and at 24 h of TOS a descending carbon profile was observed along the reactor axis (Figure 6d), with distinct D and G bands observed only at positions 1 and 2. According to our mechanism, the presence of a small amount of O_2 in the experiments acted as an inhibitor of the growth of the C-deposits, thus slowing down the dynamic of accumulation of C-deposits at the surface and, in turn, its effect on the CH_4 conversion dynamics (Figure 6c).

In conclusion, our research has unveiled novel experimental insights into the dynamics of Rh catalysts during the MDR process. We have formulated a mechanistic explanation for carbon deposition that is applicable across a broad spectrum of operational conditions. This mechanism marks a significant advancement in understanding catalyst deactivation during MDR, laying the groundwork for the rational design of catalytic materials. By employing a multi-technique approach, we demonstrated how the formation and growth of carbon aggregates on the surface affect the catalyst stability throughout the TOS. Notably, the dynamics of these surface processes are significantly influenced by the methane concentration and the CO_2/CH_4 ratio. The proposed mechanism links carbon formation and growth with catalyst activity and offers crucial insight for resolving the seeming discrepancies in existing literature regarding CO_2's kinetic role in the MDR reaction on Rh.[1a] Specifically, while the kinetics of MDR on Rh appear to be CO_2-independent even for $CO_2/CH_4 \leq 1$ under differential conditions,[15d] other studies[15b] have indicated a kinetic influence of CO_2 at high methane (CH_4) conversion rates (based on integral data) when the CO_2/CH_4 ratio is less than or equal to 1. The analysis of carbon deposition provides a resolution to this apparent contradiction. Essentially, at CO_2/CH_4 ratios of 1 or lower, carbon aggregates nucleate on the surface rapidly, affecting the observed conversion rates in a very short timeframe. Hence, the impact of CO_2 on the kinetics is an indirect consequence of carbon deposition, which partially covers the active sites. This effect does not occur within the timeframe of the catalytic cycle's turnover frequency. Therefore, it is not a kinetic effect but is associated with a deactivation phenomenon. Furthermore, the explanation provided aligns with observations that the presumed kinetic effect of CO_2 tends to disappear when even a small amount of O_2 is introduced into the feed,[15b] which in our interpretation is reconciled with the inhibition of the formation and growth of the C aggregates.

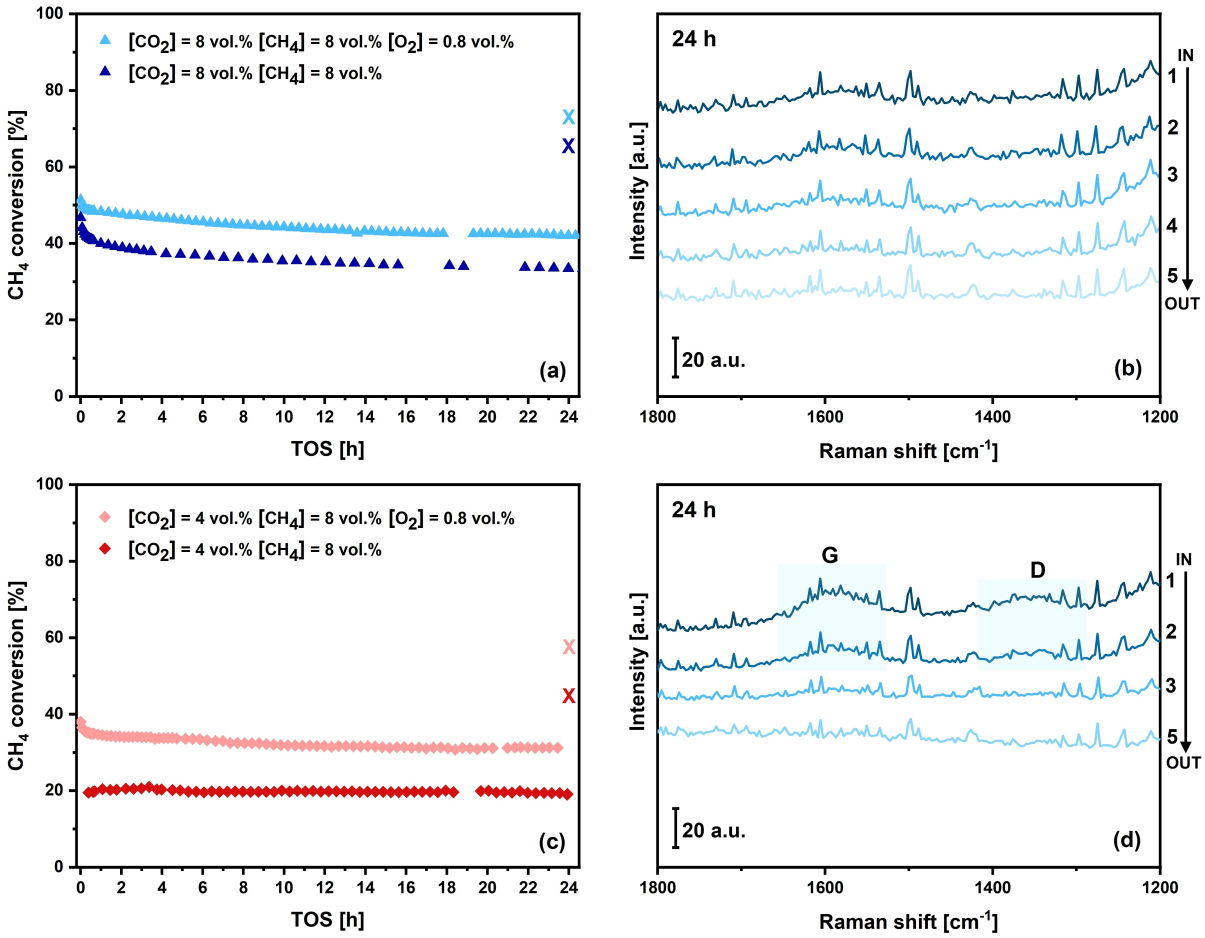

Figure 6. Methane conversion during 24 h of Methane Dry Reforming (MDR) test on a 4% Rh/Al_2O_3 catalyst, performed with and without O_2 co-feed (O_2 = 0.8 vol.%) for inlet CH_4 = 8 vol.% at (a) CO_2/CH_4 = 1, (c) CO_2/CH_4 = 0.5.%, with respective equilibrium conversion ("X" symbols). Conditions: T = 600 °C, P = 1 atm, Gas-Hourly Space Velocity (GHSV) = 1400 [L(STP)/g_{cat}/h]. (b) and (d) spatially resolved operando Raman spectra acquired during MDR at a time-on-stream (TOS) of 24 h with O_2 co-feed (0.8 vol.%) at CO_2/CH_4 = 1 (b), CO_2/CH_4 = 0.5 (d). Position 1: reactor entrance, position 5: reactor outlet, one position every 5 mm.

Acknowledgements

Financial support from the European Research Council (Grant 677423) and the National Recovery and Resilience Plan (NRRP), Mission 4 Component 2 Investment 1.3—Call for tender No. 1561 of 11.10.2022 of Ministero dell'Università e della Ricerca (MUR); funded by the European Union—NextGenerationEU—Award Number: Project code PE0000021, Concession Decree No. 1561 of 11.10.2022 adopted by Ministero dell'Università e della Ricerca (MUR), CUP D43C22003090001, according to attachment E of Decree No. 1561/2022, Project title "Network 4 Energy Sustainable Transition—NEST". B.M.W. acknowledges financial support from the Netherlands Organization for Scientific Research (NWO) for a Gravitation Program (Multiscale Catalytic Energy Conversion, MCEC). M.M. and B.M.W. acknowledge the Advanced Research Center Chemical Building Blocks Consortium (ARC CBBC) for funding.

Conflict of Interest

The authors declare no conflict of interest.

Data Availability Statement

The data that support the findings of this study are available from the corresponding author upon reasonable request.

Keywords: methane dry reforming · carbon formation · catalyst deactivation · structure-composition-performance relationship · operando spectroscopy

[1] a) M. I. Alam, R. Cheula, G. Moroni, L. Nardi, M. Maestri, *Catalysis Science, Technology* **2021**, *11*, 6601–6629; b) M. S. Fan, A. Z. Abdullah, S. Bhatia, *ChemCatChem* **2009**, *1*, 192–208.

[2] a) Y. Gao, J. Jiang, Y. Meng, F. Yan, A. Aihemaiti, *Energy Convers. Manage.* **2018**, *171*, 133–155; b) E. Le Saché, T. R.

Reina, *Prog. Energy Combust. Sci.* **2022**, *89*, 100970–100970; c) D. Wang, P. Littlewood, T. J. Marks, P. C. Stair, E. Weitz, *ACS Catal.* **2022**, *12*, 8352–8362.
[3] a) S. Arora, R. Prasad, *RSC Adv.* **2016**, *6*, 108668–108688; b) M. P. Kohn, M. J. Castaldi, R. J. Farrauto, *Appl. Catal. B* **2010**, *94*, 125–133.
[4] a) M. D. Argyle, C. H. Bartholomew, *Catalysts* **2015**, *5*, 145–269; b) X. E. Verykios, *Int. J. Hydrogen Energy* **2003**, *28*, 1045–1063.
[5] a) A. Moral, I. Reyero, C. Alfaro, F. Bimbela, L. M. Gandía, *Catal. Today* **2018**, *299*, 280–288; b) A. Navarro-Puyuelo, M. Atienza-Martínez, I. Reyero, F. Bimbela, L. M. Gandía, *Fuel* **2024**, *366*, 131285–131285; c) A. Navarro-Puyuelo, I. Reyero, A. Moral, F. Bimbela, M. A. Bañares, L. M. Gandía, *J. Ind. Eng. Chem.* **2019**, *80*, 217–226; d) D. Pakhare, J. Spivey, *Chem. Soc. Rev.* **2014**, *43*, 7813–7837.
[6] H. Y. Wang, E. Ruckenstein, *Appl. Catal. A* **2000**, *204*, 143–152.
[7] a) S. L. Leung, J. Wei, W. L. Holstein, M. Avalos-Borja, E. Iglesia, *J. Phys. Chem. C* **2020**, *124*, 20143–20160; b) C. Vogt, J. Kranenborg, M. Monai, B. M. Weckhuysen, *ACS Catal.* **2019**, *10*, 1428–1438.
[8] M. V. Martínez-Huerta, G. Deo, J. L. G. Fierro, M. A. Bañares, *J. Phys. Chem. C* **2008**, *112*, 11441–11447.
[9] A. Maghsoumi, A. Ravanelli, F. Consonni, F. Nanni, A. Lucotti, M. Tommasini, A. Donazzi, M. Maestri, *React. Chem. Eng.* **2017**, *2*, 908–918.
[10] a) U. Bentrup, *Chem. Soc. Rev.* **2010**, *39*, 4718–4730; b) I. L. C. Buurmans, B. M. Weckhuysen, *Nat. Chem.* **2012**, *4*, 873–886; c) R. Schlogl, *CATTECH* **2001**, *5*, 146–170; d) M. A. Serrer, M. Stehle, M. L. Schulte, H. Besser, W. Pfleging, E. Saraçi, J. D. Grunwaldt, *ChemCatChem* **2021**, *13*, 3010–3020; e) B. M. Weckhuysen, *Angew. Chem. Int. Ed.* **2009**, *48*, 4910–4943.
[11] A. C. Ferrari, J. C. Meyer, V. Scardaci, C. Casiraghi, M. Lazzeri, F. Mauri, S. Piscanec, D. Jiang, K. S. Novoselov, S. Roth, *Phys. Rev. Lett.* **2006**, *97*, 187401–187401.
[12] W. Li, Z. Zhou, W. Zhou, H. Li, X. Zhao, G. Wang, G. Sun, Q. Xin, *Chin. J. Catal.* **2003**, *24*, 465–470.
[13] C. H. Bartholomew, *Catal. Rev. Sci. Eng.* **1982**, *24*, 67–112.
[14] a) G. Delen, M. Monai, F. Meirer, B. M. Weckhuysen, *Angew. Chem. Int. Ed.* **2021**, *60*, 1620–1624; b) D. Fu, K. Park, G. Delen, Ö. Attila, F. Meirer, D. Nowak, S. Park, J. E. Schmidt, B. M. Weckhuysen, *Chem. Commun.* **2017**, *53*, 13012–13014.
[15] a) M. C. J. Bradford, M. A. Vannice, *Appl. Catal. A* **1996**, *142*, 73–96; b) A. Donazzi, A. Beretta, G. Groppi, P. Forzatti, *J. Catal.* **2008**, *255*, 259–268; c) J. R. Rostrupnielsen, J. H. B. Hansen, *J. Catal.* **1993**, *144*, 38–49; d) J. Wei, E. Iglesia, *J. Catal.* **2004**, *225*, 116–127.
[16] a) M. A. Pimenta, G. Dresselhaus, M. S. Dresselhaus, L. G. Cancado, A. Jorio, R. Saito, *Phys. Chem. Chem. Phys.* **2007**, *9*, 1276–1290; b) A. Sadezky, H. Muckenhuber, H. Grothe, R. Niessner, U. Pöschl, *Carbon* **2005**, *43*, 1731–1742.
[17] a) J. A. Silva, J. B. O. Santos, D. Torres, J. L. Pinilla, I. Suelves, *Int. J. Hydrogen Energy* **2021**, *46*, 35137–35148; b) S. Takenaka, M. Serizawa, K. Otsuka, *J. Catal.* **2004**, *222*, 520–531.
[18] D. Nowak, W. Morrison, H. K. Wickramasinghe, J. Jahng, E. Potma, L. Wan, R. Ruiz, T. R. Albrecht, K. Schmidt, J. Frommer, *Sci. Adv.* **2016**, *2*, e1501571–e1501571.
[19] P. K. Chu, L. Li, *Mater. Chem. Phys.* **2006**, *96*, 253–277.
[20] G. G. Tibbetts, *J. Cryst. Growth* **1984**, *66*, 632–638.
[21] a) G. F. Froment, *J. Mol. Catal. A* **2000**, *163*, 147–156; b) G. F. Froment, K. B. Bischoff, *Chem. Eng. Sci.* **1961**, *16*, 189–201; c) G. F. Froment, K. B. Bischoff, *Chem. Eng. Sci.* **1962**, *17*, 105–114.
[22] M. Maestri, D. G. Vlachos, A. Beretta, G. Groppi, E. Tronconi, *J. Catal.* **2008**, *259*, 211–222.
[23] A. Gili, L. Schlicker, M. F. Bekheet, O. Görke, D. Kober, U. Simon, P. Littlewood, R. Schomäcker, A. Doran, D. Gaissmaier, *ACS Catal.* **2019**, *9*, 6999–7011.
[24] L. Ni, K. Kuroda, L.-P. Zhou, T. Kizuka, K. Ohta, K. Matsuishi, J. Nakamura, *Carbon* **2006**, *44*, 2265–2272.
[25] a) N. Muradov, *Catal. Commun.* **2001**, *2*, 89–94; b) J. Zhang, X. Li, H. Chen, M. Qi, G. Zhang, H. Hu, X. Ma, *Int. J. Hydrogen Energy* **2017**, *42*, 19755–19775.
[26] a) B. Fidalgo, L. Zubizarreta, J. M. Bermúdez, A. Arenillas, J. A. Menéndez, *Fuel Process. Technol.* **2010**, *91*, 765–769; b) G. Zhang, Y. Dong, M. Feng, Y. Zhang, W. Zhao, H. Cao, *Chem. Eng. J.* **2010**, *156*, 519–523.
[27] L. Xu, Y. Liu, Y. Li, Z. Lin, X. Ma, Y. Zhang, M. D. Argyle, M. Fan, *Appl. Catal. A* **2014**, *469*, 387–397.

Manuscript received: May 7, 2024
Accepted manuscript online: July 3, 2024
Version of record online: ■■, ■■

Research Article

Heterogeneous Catalysis

R. Colombo, G. Moroni, C. Negri, G. Delen, M. Monai,* A. Donazzi, B. M. Weckhuysen, M. Maestri* _____ **e202408668**

Surface Carbon Formation and its Impact on Methane Dry Reforming Kinetics on Rhodium-Based Catalysts by Operando Raman Spectroscopy

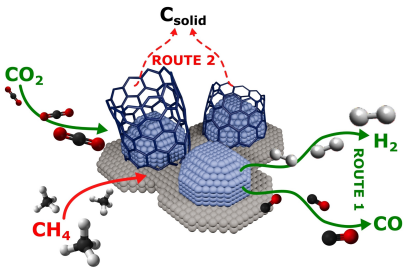

Kinetic measurements, combined with operando Raman spectroscopy and ex situ microscopy characterization provided new insights on the carbon formation pathway over Rhodium-based catalyst materials during methane dry reforming, which allowed to relate the reaction kinetics with changes in catalyst structure under true reaction conditions.